Proc Indian Natn Sci Acad **79** No. 4 December 2013 Spl. Issue, Part A, pp. 575-585

DOI: 10.16943/ptinsa/2013/v79i4/47995

Research Paper

Extended Kantorovich 3D Solution and Performance of 2D Laminate Theories for Edge Effects in Smart Piezolaminated Structures

P KUMARI[1] and S KAPURIA[2*]
[1,2]*Department of Applied Mechanics, Indian Institute of Technology Delhi, New Delhi 110 016, India*

(Received 06 March 2013; Accepted 24 March 2013)

After the recent development of an accurate semi-analytical solution based on the three dimensional (3D) piezoelasticity for the piezolaminated plates under arbitrary boundary conditions, it is now possible to assess the accuracy of two-dimensional (2D) laminate theories in predicting the boundary layer stress field in elastic and piezoelectric laminates. In this work, we assess an efficient layerwise theory, namely the improved zigzag theory (IZIGT), and its smeared counterpart (ITOT) without the layerwise description of displacements, for predicting the edge effects in the smart piezoelectric laminates under electromechanical loading. The solutions based on these 2D theories for the edge effect in piezolaminated plates under cylindrical bending is obtained from an analytical Levy-type solution for rectangular plates. It is revealed that the stresses predicted by both the 2D theories are not accurate in the close vicinity of the clamped support for pressure loading, and near the clamped, soft simply supported and free supports for electric potential loading. However, away from edges, the IZIGT yields accurate results for composite as well as highly heterogeneous sandwich plates. The ITOT, on the other hand, is not good for sandwich laminates even beyond the boundary layer.

Key Words: Zigzag Theory; Extended Kantorovich Method; 3D Piezoelasticity; Boundary Layer Effect; Composite; Sandwich; Piezolaminated Plate

1. Introduction

Composite and sandwich laminates with embedded or surface-mounted piezoelectric sensors and actuators form an important class of multifunctional (smart) structures with the ability of active vibration control, acoustic control, shape control, or damage detection (health monitoring). The widely different mechanical, electric and thermal material properties in adjacent layers in these smart laminated structures, and the geometric discontinuity at the boundaries may result in a stress field near the edge boundaries, which decay rapidly away from the edges [1]. These localized stresses are often responsible for premature delamination failure and loss of actuation/sensing authority of the piezoelectric layers. So, an accurate estimation of the boundary layer stresses has been a key issue of research since long. Analytical three-dimensional (3D) full field solutions for laminates with arbitrary edge conditions can provide valuable insight into the edge effects. Very recently, the authors [2] pioneered an accurate semi-analytical three-dimensional (3D) elasticity solution based on the powerful multi-term extended Kantorovich method (EKM) for elastic laminated panels subjected to arbitrary boundary conditions, which was shown to predict the stress field near the edges accurately. Prior to this work, the EKM, which was initially proposed by Kerr [3], had been used to analyze plates [4, 5] and shells [6, 7] under arbitrary boundary conditions, based on 2D theories only. The authors [8] further extended the method to the coupled field problem of 3D piezoelasticity solution for edge stresses in hybrid piezolaminated panels under pressure and electric potential loading. The methodology can be used to

*Author for Correspondence: E-mail: kapuria@am.iitd.ac.in

obtain accurate solutions of many boundary value problems of 3D elasticity/piezoelasticity such as the free edge stresses under tension, torsion and bending.

For practical design, analysis and optimization of smart structures, one has to use two dimensional (2D) laminate theories, since the analytical three-dimensional (3D) piezoelasticity solutions are possible only for structures of some regular geometry and shapes. A large number of 2D models have been presented for the piezoelectric laminated plate structures, a review of which is available in Ref. [9]. They can be generally classified into equivalent single layer (ESL) theories [10-12], layerwise theories (LWTs) [13] and efficient layerwise theories (ELTs) [14]. The ESL theories consider global variation of various degrees in the thickness direction of displacement fields, Thus, these theories are the most computationally efficient, but are less accurate. In the LWTs, the displacements are assumed to follow a polynomial variation across each layer of the laminate. They yield very accurate results, but the number of variables increases with the layers making them computationally inefficient.

The coupled ELT, known as the zigzag theory (ZIGT), as proposed by Kapuria and coworkers [14, 15] for hybrid plates have emerged as an excellent combination of accuracy and computational efficiency. In this theory, the inplane displacements are initially assumed to have a layerwise linear variation across the thickness, superimposed with a global third order variation. But, the number of displacement variables is finally reduced to only five, like in the smeared third order theory (TOT), by enforcing the conditions of transverse shear stress continuity at layer interfaces and zero shear traction at the top and bottom surfaces. The electric potential is assumed follow a quadratic variation across the piezoelectric layer. The accuracy of the theory has been assessed by comparing its analytical solutions for simply supported hybrid rectangular plates with the available exact 3D piezoelasticity solutions. It yields very accurate results, comparable to the LWTs even for laminates with very inhomogeneous lay-ups. However, since no boundary layer effects are observed on the simply-supported edges [16] as opposed to clamped and free edges, the assessment of 2D laminate theories for simply supported plates can at best provide an incomplete picture.

In a recent article, the authors [17] studied the boundary layer effects in Levy-type hybrid plates, using the coupled ZIGT. But in this paper, the edge effects were studied in terms of the stress resultants instead of directly the stresses, due to unavailability of reliable 3D results. In this work, we examine the accuracy of the coupled ZIGT and its smeared counterpart, the TOT, in predicting the stress field near the edges of elastic and hybrid plates in cylindrical bending with non-simply supported boundary conditions. The assessment is done in comparison with the recently developed accurate 3D piezoelasticity solution using the EKM [2, 8].

2. EKM Solution of 3D Piezoelasticity Equations for Hybrid Panel in Cylindrical Bending

2.1 Governing Equations and Boundary Conditions

We consider an infinitely long (along y axis) hybrid piezolaminated panel with span length a and thickness h. The hybrid laminate has an elastic substrate made of angle-ply composite laminas with some piezoelectric layers that are surface-bonded or embedded. The piezoelectric crystals have class mm2 symmetry and are poled along the thickness direction z. The total number of layers is L, and they are perfectly bonded to each other. It is subjected to uniformly distributed electromechanical loads applied on the bottom and top surfaces, and has arbitrary boundary conditions at the two edges at $x = 0$ and a. The 3D piezoelasticity solution of the panel presented in Ref. [8] using the EKM is briefly described here.

Using the strain-displacement, electric field-potential relations and 3D linear constitutive relations, the extended Reissner-type mixed variational principle for piezoelectric medium without body force and internal charge source can be expressed as

$$\int_V [\delta u(\tau_{xz,z} + \sigma_{x,x}) + \delta v(\tau_{yz,z} + \tau_{xy,x}) + \delta w(\sigma_{z,z} + \tau_{zx,x}) + \delta\phi(D_{x,x} + D_{z,z}) + \delta\tau_x(p_{11}\sigma_x + p_{16}\tau_{xy} + p_{13}\sigma_z + p_{18}D_z - u_{,x}) - \delta\sigma_z(w_{,z} - p_{31}\sigma_x - p_{36}\tau_{xy} - p_{33}\sigma_z - p_{38}D_z) - \delta\tau_{yz}(v_{,z} - p_{44}\tau_{yz} - p_{45}\tau_{zx} - p_{47}D_x) - \delta\tau_{zx}(u_{,z} + w_{,x} - p_{54}\tau_{yz} - p_{55}\tau_{zx} - p_{57}D_x) + \delta\tau_{xy}(p_{61}\sigma_x + p_{66}\tau_{xy} + p_{63}\sigma_z + p_{68}D_z - v_{,x}) - \delta D_x(\phi_{,x} - p_{74}\tau_{yz} - p_{75}\tau_{zx} + p_{77}D_x) - \delta D_z(\phi_{,z} - p_{81}\sigma_x - p_{86}\tau_{xy} - p_{83}\sigma_z - p_{88}D_z)]dV = 0 \quad (1)$$

where, a subscript comma denotes partial differentiation. V denotes the volume of the panel per unit width in the y direction; σ_i, τ_{ij}, D_i are normal stresses, transverse shear stresses and electric displacements; u, v, w are the displacements along x, y, z directions; ϕ is electric potential; p_{ij} denotes modified material constants. A dimensionless inplane coordinate ξ which takes values 0, 1 at $x = 0$; a; and a local thickness coordinate ζ for the kth layer which takes values 0, 1 at. The non-homogeneous boundary conditions at the top and bottom surfaces of the plate are:

$$\begin{aligned} &\text{at } z = -h/2: \ \sigma_z = -p_1, \ \tau_{yz} = 0, \\ &\quad \tau_{zx} = 0, \quad \phi = \phi_1 \text{ or } D_z = D_1 \\ &\text{at } z = h/2: \ \sigma_z = -p_2, \ \tau_{yz} = 0, \\ &\quad \tau_{zx} = 0, \quad \phi = \phi_2 \text{ or } D_z = D_2 \end{aligned} \quad (2)$$

The interfaces between the piezoelectric layers and the elastic layers are taken as grounded for effective actuation/sensing. For such interfaces $n_q (q = 1, ..., L_a)$, the electric potential is prescribed as

$$[\phi|_{\zeta=1}]^{(n_q)} = 0, \quad q = 1,....,L_a \quad (3)$$

The equilibrium and the compatibility conditions at the kth interface between adjacent layers are:

$$[(u, v, w, \sigma_z, \tau_{yz}, \tau_{zx}, \phi, D_z|_{\zeta=1}]^{(k)} = [(u, v, w, \sigma_z, \tau_{yz}, \tau_{zx}, \phi, D_z|_{\zeta=0}]^{(k+1)} \quad (4)$$

for $k = 1, ... L–1$; except for D_z for the interfaces $k = n_q$, $q = 1, ... L_a$. The D_z is discontinuous for the interfaces. For such surfaces, the continuity condition for D_z is to replaced by Eq. (3). The boundary conditions at the edges $x = 0$ and 1 can be arbitrary e.g. simply supported, clamped and free.

2.2 Solution Using the EKM

The solution of the field variables, $D_z = [u\ v\ w\ \sigma_x\ \sigma_z\ \tau_{xy}\ \tau_{yz}\ \tau_{zx}\ \phi\ D_x\ D_z\ ]^T$ is constructed as a sum of n terms of product of two separable functions in the inplane (x) and thickness (z) directions, which is superimposed with a solution satisfying identically the nonhomogenous boundary conditions of applied pressure and electric potential/charge at the top and bottom surfaces:

$$X_l(\xi, \varsigma) = \sum_{i=1}^{n} f_l^i(\xi) g_l^i(\varsigma) + \delta_{l5}[p_a + zp_d] + \delta_{l9}\bar{g}_9 \text{ for } l = 1,2,....,11. \quad (5)$$

wherein, $f_l^i(\xi)$ and $g_l^i(\varsigma)$ are unknown univariate functions of ξ and ζ to be determined iteratively, satisfying all homogenous boundary conditions. The repeated index l does not mean summation here δ_{lm} is Kronecker's delta, $p_a = -(p_1 + p_2)/2$ and $p_a = -(p_2 - p_1)/h$. The solution $\bar{g}_9$ for nonhomogenous boundary condition of ϕ is given by

$$\bar{g}_9 = \begin{Bmatrix} \phi_1(1-\varsigma) & \text{for} \quad k = 1 \\ \phi_2\varsigma & \text{for} \quad k = L \end{Bmatrix} \quad (6)$$

In the first iteration step, functions $f_l^i(\xi)$ are assumed, the functions $g_l^i(\varsigma)$ are partitioned into a column vector $\bar{G}$ of those eight variables that appear in the boundary conditions given in Eq. (2) and column vector $\hat{G}$ consisting of the remaining. Substituting the variable X_l in Eq. (1), integrating over x direction and considering that the variations $g_l^i(\varsigma)$ are arbitrary,

the coefficient of $\delta g_l^i(\varsigma)$ l = 1, 2, ..., 11 are equated to zero individually. This results in the following set of differential-algebraic equations for $\delta g_l^i(\varsigma)$.

$$\begin{aligned} M\bar{G}_{,\varsigma} &= \bar{A}\bar{G} + \hat{A}\hat{G} + \bar{Q}_p + \bar{Q}_e \ (8n \text{ ODEs}); \\ K\hat{G} &= A\bar{G} + Q_p \ (3n \text{ algebric equations}) \end{aligned} \tag{7}$$

where, M, $\bar{A}$, $\hat{A}$, K and $\tilde{A}$ are $8n\times 8n$, $8n\times 8n$, $8n\times 3n$, $3n\times 3n$ and $3n\times 8n$ matrices, $\bar{Q}_p$, $\bar{Q}_e$ and $\tilde{Q}_p$ are load vectors of size $8n$, $3n$ and $8n$, respectively. Solving the system of algebraic equations for $\hat{G}$ and substituting back the solution into first order ordinary differential equations (ODEs) yields a set of $8n$ non-homogenous first order ODEs with constant coefficients, which are solved in close-form, satisfying the homogeneous version of the boundary conditions (2) and interface continuity conditions given by Eqs. (3) and (4).

In the next step, the solution of the first step is taken as the known approximate solution for $g_l^i(\varsigma)$ and considering variations $\delta f_l^i(\xi)$ are arbitrary. Following the same procedure as discussed above, following system of differential-algebraic equations for $f_l^i(\xi)$ is given as

$$\begin{aligned} N\bar{F}_{,\xi} &= \bar{B}\bar{F} + \hat{B}\hat{F} + \bar{P}_m \ (8n \text{ ODEs}); \\ L\hat{F} &= \tilde{B}\bar{F} + \tilde{P}_m \ (3n \text{ algebric equations}) \end{aligned} \tag{8}$$

where, N, $\bar{B}$, $\hat{B}$, L and $\tilde{B}$ are $8n\times 8n$, $8n\times 8n$, $8n\times 3n$, $3n\times 3\,n$ and $3n\times 8n$ matrices respectively, $\bar{P}_m$ and $\tilde{P}_m$ are load vectors of size $8n$, $3n$ respectively. Equation (8) is solved similarly. Starting with initial trial functions in x-direction, the functions in z and x directions are solved alternatively, till the convergence is achieved.

3. Analytical Solution of Levy-Type Hybrid Plate using 2D Theories

3.1 Approximations for Field Variables

Consider a rectangular hybrid laminated plate (Fig. 1) with two opposite (at x = 0; a) simply supported

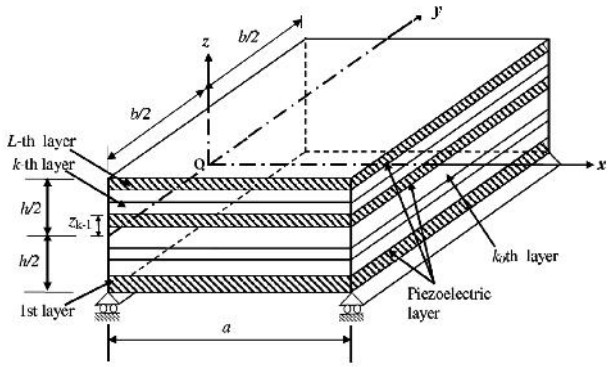

Fig. 1: Geometry of a hybrid plate

and the remaining two having arbitrary boundary conditions. In the coupled improved zigzag theory (IZIGT) [15], the linear constitutive equations of the piezoelectric laminate with the usual assumption of negligible transverse normal stress ($\sigma_z \simeq 0$) are considered here. ϕ is approximated as a piecewise quadratic between n_ϕ points at $z = z_\phi^j$ across the thickness of the laminate:

$$\phi(x,y,z) = \psi_\phi^j(z)\phi^j(x,y) + \psi_c^q(z)\phi_c^q(x,y) \tag{9}$$

where, ϕ^j denotes the electric potential at the piezoelectric layer sensors/interfaces at $z = z_\phi^j$ with $j \in [1, 2, ..., n_\phi]$. ϕ_c^q denotes the quadratic component of electric potential at $z = (z_\phi^q + z_\phi^{q+1})/2$ with $q \in [1, 2, ..., n_\phi - 1]$. Thus $z = z_\phi^j$ is the z-coordinate of jth point from bottom for discretising ϕ. The summation convention is used for repeated indices j and $q \cdot \psi_\phi^j(z)$ is a piecewise linear function and $\psi_c^q(z)$ is a quadratic function, given by

$$\psi_c^q(z) = \begin{Bmatrix} 4\,(z_\phi^{q+1} - z)\,(z - z_\phi^q)/(z_\phi^{q+1} - z_\phi^q)^2 \\ \text{if } z_\phi^q \le z \le z_\phi^{q+1} \\ 0 \qquad \text{otherwise} \end{Bmatrix} \tag{10}$$

The approximation of the deflection w accounts for the transverse deformation due to the transverse electric field. Integrating the constitutive equation for ε_z after neglecting the contribution of elastic

compliance gives

$$w(x,y,z) = w_0(x,y) - \bar{\psi}_{\varphi}^{j}(z)\phi^{j}(x,y) - \bar{\psi}_{c}^{q}(z)\phi_{c}^{q}(x,y) \tag{11}$$

where, $\bar{\psi}_{\varphi}^{j}(z) = \int_0^z d_{33}\psi_{\phi,z}^{j}(z)dz$ and $\bar{\psi}_{c}^{q}(z) = \int_0^z d_{33}\psi_{c,z}^{q}(z)dz$. The inplane displacements u_x and u_r are approximated in the thickness direction as a combination of a third-order variation in z over the entire laminate thickness and a layerwise linear variation with discontinuity in slopes $u_{x,z}$ and $u_{y,z}$ at the layer interfaces. Using the conditions of u continuity of and of the transverse shear stresses τ at the layer interfaces and four shear traction-free conditions at the top and bottom surfaces, finally u can be expressed as

$$u(x,y,z) = u_0(x,y) - zw_{0_d}(x,y) + R^{k}(z)\psi_0(x,y) + R^{kj}(z)\phi_d^{j} \tag{12}$$

where $u = [u_x\ u_y]$; $u_0 = [u_{0x}\ u_{0y}]$; $w_{0_d} = [u_{0,x}\ u_{0,y}]$; $\psi_0 = [\psi_{0x}\ \psi_{0y}]$; $\phi_d^{j} = [\phi_q^{j}, \phi_y^{j}]^T$ and $R^k(z)$ and $R^{kz}(z)$ are 2 x 2 matrices of layerwise functions of z which depends on material properties and lay-up. The smeared improved third order theory (ITOT) has the same global variation of the inplane displacements as the IZIGT, but there are no layerwise terms. Thus, u for the ITOT can be expressed in the form of Eq. (12) where $R^k(z)$ will have only global functions of z, and no layerwise functions.

3.2 Governing Equations

Substituting the expression of deflections, electric potential, strains and electric displacement in the principle of virtual work, and applying Greens theorem, wherever required, yields the coupled equations of equilibrium for the laminated piezoelectric plate as

$$\begin{aligned}
&N_{x,x} + N_{xy,y} = 0, \quad N_{xy,x} + N_{y,y} = 0, \ M_{x,xx} \\
&+2M_{xy,xy} + M_{y,yy} + P_3 = 0 \\
&P_{x,x} + P_{yx,y} - Q_x = 0, \quad P_{xy,x} + P_{y,y} - Q_y = 0, \\
&\tilde{Q}_{x,x}^{q} + \tilde{Q}_{y,y}^{q} + \tilde{H}_{x,x}^{q} + \tilde{H}_{x,x}^{q} - \tilde{G}^{q} = 0 \\
&Q_{x,x}^{j} + Q_{y,y}^{j} + H_{x,x}^{j} + H_{y,y}^{j} - S_{x,xx}^{j} - 2S_{xy,yx}^{j} \\
&-S_{y,yy}^{j} - G^{j} + P_{\phi}^{j} = 0, \quad \text{for } j = 1,2,...n_{\phi} \\
&\text{and } q = 1,2,...n_{\phi}^{q}.
\end{aligned} \tag{13}$$

where, $P_3 = p_z^1 + p_z^2$ and $\mathrm{P}_{\phi}^{\mathrm{j}} = -p_z^1\bar{\psi}_{\phi}^{j}(z_0) - p_z^2\bar{\psi}_{\phi}^{j}(z_L) + D_{z_L}\delta_{jn\phi} + D_{z_0}\delta_{j1} + q_{j_i}\delta_{jj_i}$, p_z^2, p_z^1 are mechanical load applied at the top and bottom of the plate; $(D_{z_L}, D_{z0}), q_{j_i}$ are electric displacements and jump in the electric displacements; δ_{ij} is Kronecker's delta. The variationally consistent boundary conditions on edges can be expressed as the prescribed values of one of the factors of each of the following products:

$$\begin{aligned}
&u_{0_n}N_n,\ u_{0s}N_{ns},\ w_0(V_n + M_{ns,s}),\ w_{0,n}M_n, \\
&\psi_{0_n}P_n,\ \psi_{0_s}P_{ns},\ \phi_c^q(H_n^q - V_{\phi_n}^q), \\
&\phi^j(H^j - V_{\phi_n}^j - S_{ns,s}^j),\ \phi_{,n}^j S_n^j \\
&\text{and at corners } s_i\text{: } w_0(s_i)\Delta M_{ns}(s_i), \\
&\phi^j(s_i)\Delta S_{ns}^j(s_i)
\end{aligned} \tag{14}$$

where, N, M, P, Q, and V denote inplane stress resultants, bending moments, higher order moments, shear resultants, and transverse shear resultants; S^j, $\bar{Q}^j$, $\tilde{Q}^q$, H^j, $\tilde{H}^q$, G^j, $\tilde{G}^q$ electromechanical stress resultants. Using the mixed formulation approach, these governing differential equations are expressed in terms of displacements, stress resultants, electric potential and electric displacement resultants that appear in the boundary conditions at the arbitrary edges.

Thus, the solution in the y direction is developed in terms of 12 mechanical and 2 n_{ϕ}^{q} electrical primary variables given by

$$\begin{aligned}
X_m = [&u_{0x_m}\, u_{0y_m}\, w_0\, w_{0,y_m}\, \psi_{0x_m}\, \psi_{0y_m}\, N_{y_m}\, N_{xy_m} \\
&(V_{y_m} + M_{xy,x_m})\, M_{y_m}\, P_{y_m}\, P_{xy_m}\, (Q_y^q + H_y^q)_m \phi_{c_m}^q]^{\mathrm{T}}
\end{aligned}$$

Expanding the solution in terms of Fourier series along the x-direction meeting the simply supported ends, the governing differential equations reduce to a

system $12+2n_\phi^q$ first order ODEs and n_ϕ algebraic equations for variables X_m for each Fourier component m:

$$H^m X_{m,y} = K^m X_m + P^m + C^m \phi^m \tag{15}$$

$$F^m \phi^m = H_\phi^m X_{m,y} + K_\phi^m X_m - P_\phi^m \tag{16}$$

where, H^m, K^m, P^m, C^m, F^m, H_ϕ^m, K_ϕ^m and P_ϕ^m are the coefficient matrices. Equation (16) is an algebraic equation. In a general actuation-sensory response, some of the piezoelectric layers act as sensors wherein the induced electric potential is unknown, and others as actuators where voltage is prescribed Φ^m is partitioned into a set of unknown (sensor) output voltages Φ_a^m at locations $z = z_\phi^j$ where Φ^m is not prescribed and a set of known input actuation voltages Φ_a^m at the actuated surfaces $z = z_\phi^{j_i}$. The corresponding matrices F^m, H_ϕ^m, K_ϕ^m and P_ϕ^m are also partitioned as

$$\begin{bmatrix} F_{ss}^m & F_{sa}^m \\ F_{sa}^m & F_{aa}^m \end{bmatrix} \begin{bmatrix} \Phi_s^m \\ \Phi_a^s \end{bmatrix} = \begin{bmatrix} H_{\phi s}^m \\ H_{\phi a}^m \end{bmatrix} X_{m,y} + \begin{bmatrix} K_{\phi s}^m \\ K_{\phi a}^m \end{bmatrix} X_m - \begin{bmatrix} P_{\phi s}^m \\ P_{\phi a}^m \end{bmatrix} \tag{17}$$

which is solved for Φ_s^m and substituting Φ_s^m into the partitioned Eq. (15) yields

$$\tilde{H}^m X_{m,y} = \tilde{K}^m X_m + \tilde{P}^m \tag{18}$$

where, $\tilde{H}^m$, $\tilde{K}^m$ and $\tilde{P}^m$ are the modified matrices. It's solution is obtained in close form as in Sec. 2.2.

4. Numerical Results

To obtain the cylindrical bending behaviour in the Levy-plate model, a plate with a large value of a/b under an electromechanical loading of sinusoidal variation along x direction and a constant variation in y-direction is considered and the results are reported for the mid section at $x = a/2$. The equivalence of the coordinate systems for the two solutions are given in Fig.2 Since the effective span in this case is b, the span to thickness ratio is redefined as $S = b/h$. For this study, the effective span b is taken as 1 m.

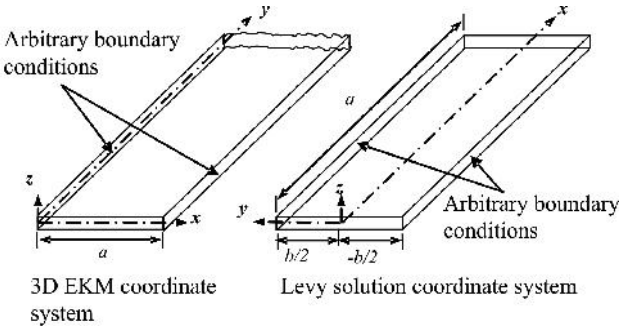

Fig. 2: Coordinate systems of EKM and Levy solutions

The numerical results are presented for plates of three configurations: Graphite-epoxy (Gr/Ep) composite plate (a), soft-core sandwich (b) with faces of Gr/Ep and hybrid sandwich plate (c) integrated with piezoelectric fiber reinforced composite (PFRC) layers at the top and bottom, as shown in Fig. 3. The properties of Gr/Ep, soft core and PFRC are given in Table 1.

4.1 Elastic Laminated Panels

The panels are subjected to a uniform pressure load $p_z^2 = p_0 \sin(\pi x/a)$ on the top surface. The results are nondimensionalized as $\bar{w} = wY_0 / p_0 h S^4$; $(\bar{\sigma}_y, \bar{\tau}_{yz}) = (\sigma_y, S\tau_{yz})/p_0 S^2$ with $S = b/h$ and $Y_0 = 10.3$ GPa. To arrive at an appropriate value of a/b for cylindrical bending response, a convergence study is conducted in Table 2 by using the results for a/b = 10, 20, 40 and 50. It is seen that very good convergence is achieved with $a/b = 50$ for panels (a) and (b). Also, whether a sinusoidal variation of pressure in the x direction is appropriate for this study is checked by comparing these results with those for a uniform pressure variation along the x-direction. Converged results for the uniform pressure load are

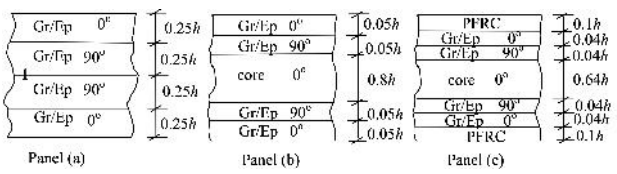

Fig. 3: Laminate configurations of elastic and hybrid panels

Table 1: Material constants

	Y_1	Y_2	Y_3	G_{23}	G_{13}	G_{12}	v_{12}	v_{13}	v_{23}
Gr/Ep	181	10.3	10.3	2.87	7.17	7.17	0.28	0.28	0.33
Core	0.276	0.276	3.45	0.1104	0.414	0.414	0.25	0.02	0.02
PFRC	38.87	13.68	13.20	3.0148	4.3541	4.3699	0.3108	0.4179	0.2007
	d_1	d_{32}	d_{33}	d_{24}	d_{15}	η_{11}	η_{22}	η_{33}	
PFRC	-263	-263	485	0	0	29.769	29.769	24.403	

Units: Young's moduli Y_1 and shear moduli G_{ij} in GPa; piezoelectric strain coefficient d_{ij} in pm/V; electric permittivities η_{ij} in nF/m

Table 2: Convergence study of Levy solution for panel (a) under CS boundary condition (S=5)

	a/b=10			*a/b*=20		
	$\bar{w}$	$\bar{\sigma}_y$	$\bar{\tau}_{yz}$	$\bar{w}$	$\bar{\sigma}_y$	$\bar{\tau}_{yz}$
(*y/b, z/h*)	(0, 0)	(-0.5, -0.5)	(-0.5, 0)	(0, 0)	(-0.5, -0.5)	(-0.5, 0)
UDL*	-2.0120	-2.6186	-0.11995	-2.0118	-2.6178	-0.1199
SL**	-2.0092	-2.6163	-0.1197	-2.0113	-2.6186	-0.1199
	a/b=40			*a/b*=50		
	$\bar{w}$	$\bar{\sigma}_y$	$\bar{\tau}_{yz}$	$\bar{w}$	$\bar{\sigma}_y$	$\bar{\tau}_{yz}$
UDL*	-2.0105	-2.6156	-0.1199	-2.0094	-2.6141	-0.1199
SL**	-2.0119	-2.6191	-0.1199	-2.0119	-2.6192	-0.1199

*Uniform distributed pressure loading in x direction; ** Sinusoidal pressure loading in x direction

Table 3: Comparison of Levy solutions for uniform and sinusoidal loading for a long hybrid panel (c) (CHD-SSP boundary condition, S=5)

	Pressure load case				
	$\bar{w}$	$\bar{\sigma}_y^p$	$\bar{\sigma}_y^c$	$\bar{\tau}_{yz}$	$\bar{\phi}$
(*y/b, z/h*)	(0,0)	(-0.5,-0.5)	(-0.5,-0.36-)	(-0.5,-0.4)	(-0.5,0.5)
UDL	-2.579	-3.5971	5.4387	-2.9369	-19.890
SL	-2.598	-3.6055	5.4528	-2.9454	-19.938
	Potential load case				
	$\bar{w}$	$\bar{\sigma}_y^p$	$\bar{\sigma}_y^c$	$\bar{\tau}_{yz}$	$\bar{\phi}$
(*y/b, z/h*)	(0,0)	(-0.45,-0.5)	(0.45,-0.36-)	(-0.45,-0.4)	(-0.45,0.5)
UDL	2.2900	120.315	-88.168	19.522	-25.060
SL	2.2909	120.320	-88.177	19.532	-25.058

obtained with M = 99. It is observed from Table 2 that the results at the mid span (x = a/2) for the sinusoidal variation match with the converged results for the uniform variation for at least three significant digits. All subsequent results are, therefore, presented with the sinusoidal pressure variation, and considering a/b = 50.

In Fig. 4, the longitudinal variations of transverse deflection $\bar{w}$, inplane stress $\bar{\sigma}_x$ and transverse shear stress $\bar{\tau}_{yz}$ are plotted for a cantilever (CF) cross-ply composite panel (a) for S = 5 and 10. The variations predicted by the ZIGT and TOT are compared with those obtained using the 3D elasticity based EKM solution. It is observed that the results of the 2D theories are in good agreement with the 3D elasticity solution, except for the stresses in the vicinity of the clamped boundary. The transverse shear stress is particularly poorly predicted near the clamped edge, the ZIGT yielding marginally better results among the two. Similar comparison for the sandwich panel (b) presented in Fig. 5 reveals that (i) the error in the stresses near the clamped boundary is also larger for the sandwich panel than the composite one, and (ii)

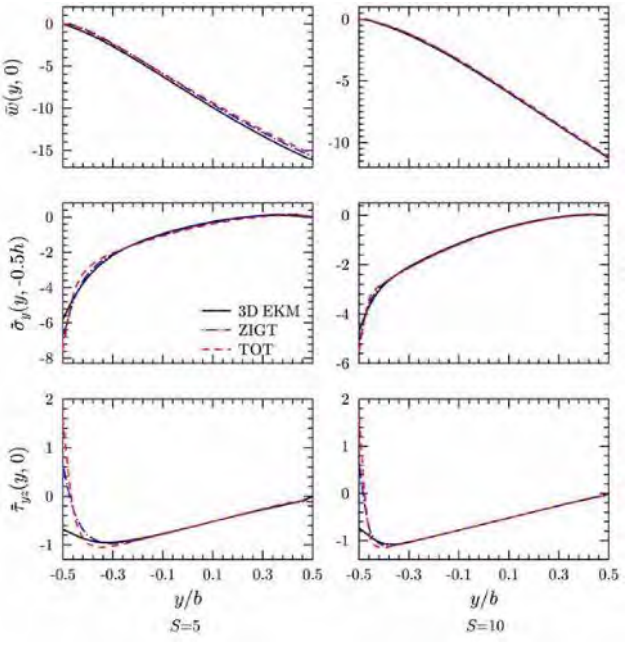

Fig. 4: Longitudinal variations of deflection and stresses for cross-ply composite panel (a) with CF boundary condition

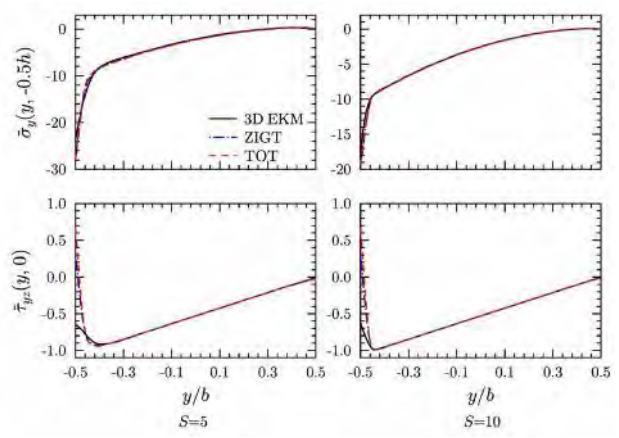

Fig. 5: Longitudinal variations of stresses for cross-ply sandwich panel (b) with CF boundary condition

this error is in general larger in the TOT than the ZIGT. Similar trends are observed from Fig. 6 for the sandwich panel under clamped-simply supported (CS) boundary conditions, and the difference between the ZIGT and TOT predictions of stresses near the clamped boundary is distinctly bigger in this case. The through-thickness distributions of the displacement $\bar{v}$, inplane stress $\bar{\sigma}_y$ and transverse shear stress $\bar{\tau}_{yz}$ are presented in Fig. 7 for panels (a) and (b) respectively, for CS boundary condition. The ZIGT results are in close agreement with 3D-EKM even near the edges while TOT results are not in good agreement. Fig. 7 reveals that layerwise variation of the displacement with slope discontinuity at the interfaces and the layerwise variation of stresses are well predicted by the ZIGT away from the non-simply supported boundary.

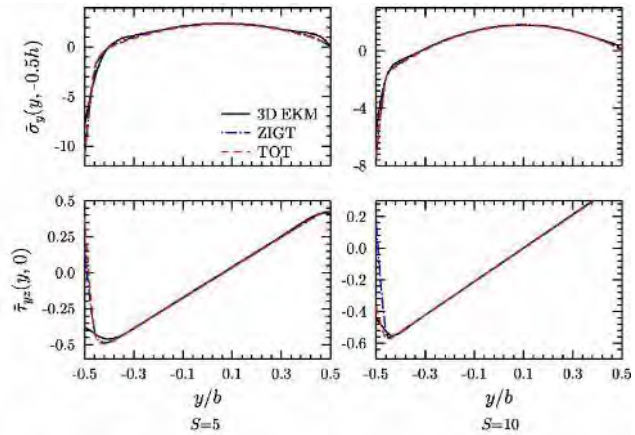

Fig. 6: Longitudinal variations of stresses for cross-ply sandwich panel (b) with CS boundary condition

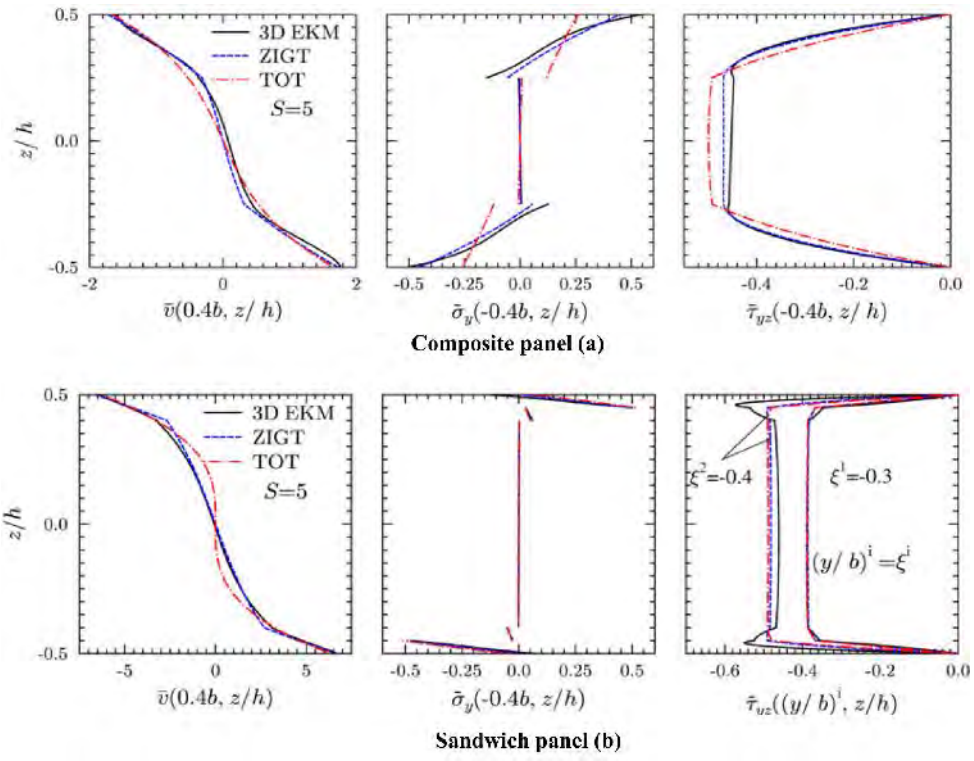

Fig. 7: Through-thickness distributions of $\bar{v}$, $\bar{\sigma}_y$ and $\bar{\tau}_{yz}$ for composite panels (a) and (b) with CS boundary condition

4.2 Hybrid Piezolaminated Panels

The response is obtained for the following two load cases:

1. Pressure $p_z{}^2 = p_0 \sin(\pi x/a)$ applied on the top surface, with open circuit condition at the top and close circuit condition at the bottom surface.

2. Actuation potential applied to the both top and bottom surfaces, $\phi^1 = \phi^{n_\phi} = \phi_0 \sin(\pi x/a)$.

Nondimensionalized parameters are as follows:

Load case 1:

$$(\bar{v}, \bar{w}, \bar{\phi}) = (S100v, 100w, 10\phi d_0 S^2) Y_0 / p_0 h S^4;$$
$$(\bar{\sigma}_y, \bar{\tau}_{yz}, \bar{D}_z) = (\sigma_y, S\tau_{yz}, D_z/d_0)/p_0 S^2$$

Load case 2 :

$$(\bar{v}, \bar{w}) = (Sv, w)/S^2 d_0 \phi_0;$$
$$(\bar{\sigma}_y, \bar{\tau}_{yz}, \bar{D}_z) = (\sigma_y, S\tau_{yz}, D_z/100d_0) h/Y_0 d_0 \phi_0$$

where, Y_0 = 10.3 GPa, d_0 = 100 x 10^{-12}mV^{-1}. The boundary conditions of an edge are identified by both mechanical and electric boundary conditions. Thus, a hard clamped (CH) edge under open circuit condition (D) is denoted as CHD. The plates are denoted in terms of their boundary conditions at the edges at $y = \mp b/2$. For example, a CHP-FP plate means a plate with boundary condition CHD at $y = -b/2$ and FP (free edge under close circuit condition) at $y = b/2$.

Based on a convergence study, the value of a/b to model the cylindrical bending response is taken 50 as in the elastic case. To check whether a sinusoidal variation of pressure and electric potential in the x direction will yield an accurate response for the cylindrical bending case, the convergence for the uniform pressure and potential loadings are compared in Table 3 with those for the sinusoidal variation. It is observed that the results at the mid-span ($x = a/2$) for the sinusoidal variation match with the converged results for the uniform variation for three significant digits. All subsequent results are, therefore, presented

with the sinusoidal variation.

In Fig. 8, the longitudinal variations of displacements $\bar{u}$, $\bar{w}$, inplane stress $\bar{\sigma}_x$, transverse shear stress $\bar{\tau}_{yz}$ and electric potential $\bar{\phi}$ are plotted for a thick clamped simply-supported (CHD-SSP) sandwich panel (c) with S = 5 under the pressure load case. The variations predicted by the IZIGT and ITOT are compared with those obtained using the 3D piezoelasticity based EKM solution. The converged solution of the EKM is taken for the purpose. It is observed that the results of IZIGT are in very good agreement with the 3D piezoelasticity solution, except for the stresses in the close vicinity of the clamped boundary. In case of ITOT, not only the predicted stresses deviate more from the 3D EKM solution, but even the predicted displacements are highly erroneous. The prediction for the induced electric potential by the ITOT is also the erroneous and inferior to the IZIGT.

The variations of the displacements (in Fig. 10 only), stresses and the electric displacement $\bar{D}_z$ under the potential load case are plotted in Figs. 9 and 10 for the CHP-FP and CHP-SSP boundary conditions, respectively. It is seen that the IZIGT results are

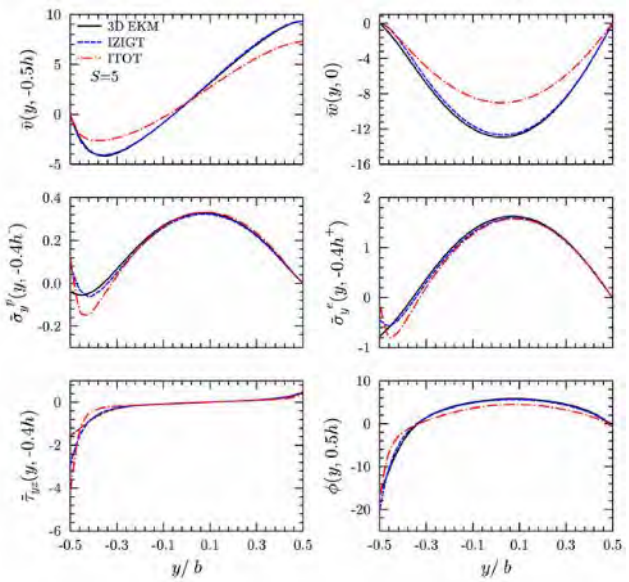

Fig. 8: Longitudinal variations of deflection and stresses for sandwich panel (c) with CHD-SSP boundary condition under pressure load

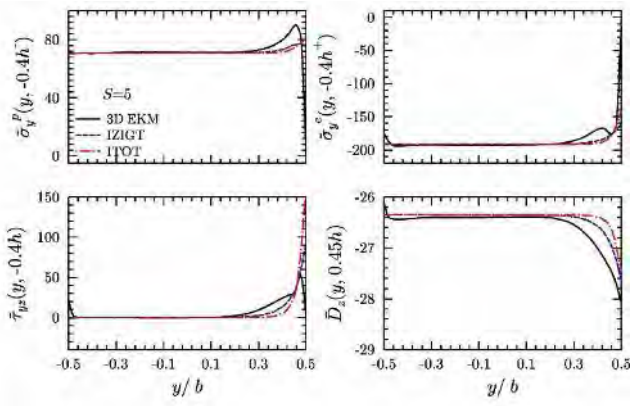

Fig. 9: Longitudinal variations of stresses and transverse electric displacement for thick hybrid sandwich panel (c) with CHP-FP boundary condition under potential loading

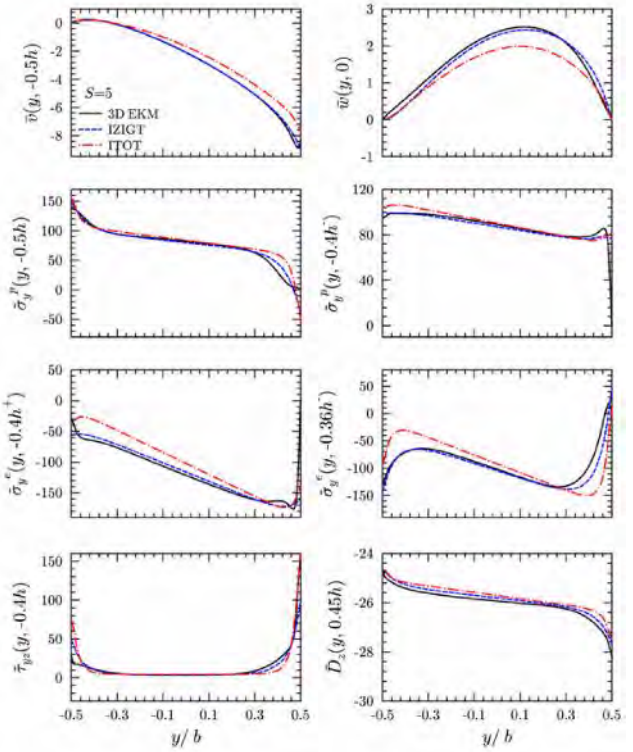

Fig. 10: Longitudinal variations of displacements, stresses and transverse electric displacement for thick hybrid sandwich panel (c) with CHP-SSP boundary condition under potential loading

superior to the ITOT for both cases and are generally accurate except for the stresses $\bar{\sigma}_y$ and $\bar{\tau}_{yz}$ in the close vicinity of supports. Similar to the pressure load case, the error in the ITOT is more significant in the

CHP-SSP case than the cantilever one. It may be noted that in the 2D plate theories, the boundary conditions related to stresses (e.g. zero normal and shear stresses at the free boundary and zero inplane stresses at the simply-supported boundary) are satisfied only in terms of stress resultants and not strictly in terms of stresses. Nevertheless, it can be seen from Fig. 8 that, under pressure loading, stresses predicted by both the 2D theories satisfy the boundary conditions at the free as well as simply supported edges. This, however, does not happen in the potential load case, as can be seen from Figs. 9 and 10. In this case, both theories predict very large values for $\bar{\sigma}_y$ and $\bar{\tau}_{yz}$ at the edges where they are supposed to be zero.

5. Conclusions

It has been found that the stresses predicted by both the 2D theories, IZIGT and ITOT, are not accurate in the close vicinity of the clamped (CH) support in the pressure load case, and near the CH, soft-simply supported (S) and free (F) supports in case of potential loading. The stresses predicted by the 2D theories in the potential load case do not satisfy the zero stress conditions at the S and F supports. However, away from supports, the IZIGT yields accurate results for hybrid composite as well as highly heterogeneous sandwich plates. The ITOT, on the other hand, is not good for sandwich laminates even away from the boundary layer.

References

1. Mittelstedt C and Becker W Free-edge effects in composite laminates *App Mech Rev* **60** (2007) 217-244
2. Kapuria S and Kumari P Multi-term extended Kantorovich method for three dimensional elasticity solution of laminated plates *J Appl Mech Trans ASME* **79** (2012) 061018 1-9
3. Kerr A D An extension of the Kantorovich method *Quart Appl Math* **4** (1968) 219-229
4. Naumenko K, Altenbach J, Altenbach H and Naumenko V K Closed and approximate analytical solutions for rectangular Mindline plates *Acta Mech* **147** (2001) 153-172
5. Aghdam M M and Mohammadi M Bending analysis of thick orthotropic sector plates with various loading and boundary conditions *Compos Struct* **88** (2009) 212-218
6. Alijani F and Aghdam M M A semi-analytical solution for stress analysis of moderately thick laminated cylindrical shells with various boundary conditions *Compos Struct* **89** (2009) 534-550
7. Bigdeli A and Aghdam M M A semianalytical solution for the bending of clamped laminated doubly curved or spherical panels *J Mech Mater Struct* **5** (2010) 855-873
8. Kapuria S and Kumari P Extended Kantorovich method for coupled piezoelasticity solution of piezolaminated plates showing edge effect *Proc R Soc A* **469** (2013) 20120565 1-19
9. Carrera E F, Brischetto S and Cinefra M Variable kinematics and advanced variational statements for free vibration analysis of piezoelectric plates and shells *Comput Modelling Engng Sc* **65** (2010) 259-341
10. Fernandes A and Pouget J Structural response of composite plates equipped with piezoelectric actuators *Comput Struct* **84** (2006) 1459-1470
11. Polit O and Bruant I Electric potential approximations for an eight node plate finite element *Comput Struct* **84** (2006) 1480-1493
12. Chattopadhyay A and Gu H Coupled piezoelectric mechanical model for smart composite laminates *AIAA J* **37** (1999) 1633-1638
13. Saravanos D A Layerwise mechanics and finite element for the dynamic analysis of piezoelectric composite plates *Int J Solids Struct* **34** (1997) 359-378
14. Kapuria S A coupled zig-zag third order theory for piezoelectric hybrid cross-ply plates *J Appl Mech Trans ASME* **71** (2004) 604-614
15. Kapuria S and Kulkarni S D Static electromechanical response of smart composite/sandwich plates using an efficient finite element with physical and electric nodes *Int J Mech Sci* **51** (2009) 1-20
16. Karama M, Touratier M and Idlbi A An evaluation of the edge solution for a higher-order laminated plate theory *Compos Struct* **25** (1993) 495-502
17. Kapuria S and Kumari P Boundary layer effects in Levy-type rectangular piezoelectric composite plates using a coupled efficient layerwise theory *Euro J Mech A/Solids* **36** (2012) 1-19.